Proceedings of the Eighteenth International Conference on
Civil, Structural and Environmental Engineering Computing
Edited by: P. Iványi, J. Kruis and B.H.V. Topping
Civil-Comp Conferences, Volume 10, Paper 9.3
Civil-Comp Press, Edinburgh, United Kingdom, 2025
ISSN: 2753-3239, doi: 10.4203/ccc.10.9.3

Wake Structures in Yawed Turbines: An LES Perspective

H. Kim, M. Shokati and S. Lee

Department of Aerospace Engineering, Korea Advanced Institute of Science and Technology (KAIST), Daejeon, South Korea

Abstract

Yaw-based wake steering has emerged as a promising approach for enhancing wind farm performance by redirecting turbine wakes. Despite its potential, the detailed dynamics and evolution of the curled wake structure resulting from rotor yaw remain insufficiently characterized. This study investigates the wake behavior behind a wind turbine subjected to a range of yaw angles under uniform inflow conditions, utilizing large-eddy simulation (LES) to capture the flow features. The NREL 5MW reference wind turbine is represented using a rotating actuator disk model to resolve the deformation process of the curled wake. Results indicate that the vertical asymmetry in the wake is primarily driven by the interaction between the global rotation of the wake and a pair of counter-rotating vortices induced by the yawed rotor. The yaw angle significantly alters the shape and path of the wake, although these effects progressively diminish with increasing downstream distance.

Keywords: NREL 5 MW turbine, wind turbine wake, large-eddy simulation, actuator disk model, wake dynamics, wake redirection, yaw control.

1 Introduction

The rotor wake from wind turbines affects wind farm performance by creating velocity deficits and turbulence, reducing power output and increasing loads on downstream turbines [1]. Yaw control is used to redirect the wake and mitigate these effects but can reduce the yawed turbine's power due to wind misalignment. Accurate prediction of the curled wake is key to optimizing total farm output [2], yet wake deflection varies non-linearly with yaw, producing a complex, three-dimensional structure. Previous studies have identified a counter-rotating vortex pair (CVP) as a defining feature in yawed wakes. Howland et al. [3] first reported the CVP, with Bastankhah and Porté-Agel [4] confirming its role in wake dynamics. This feature has since formed the basis of several wake modeling efforts [5]. Global wake rotation has also been shown to influence deformation. Howland et al. [3] observed top-down asymmetry in yawed wakes, while Bastankhah et al. [4] linked vertical shifts to the CVP, and Schottler et al. [6] noted opposite displacements for turbines with reversed rotation. Kleusberg et al. [7] further demonstrated that the CVP weakens at higher tip-speed ratios.

Turbulent mixing plays a key role in wake recovery and shape distortion [8]. Lin and Porté-Agel [9] reported asymmetrical turbulence intensity in yawed wakes, and Bartl et al. [10] observed elevated turbulent energy along the wake edges. Hulsman et al. [11] identified a skewed ring-like structure in the wake region. Despite these contributions, the detailed evolution of the curled wake remains only partially understood. This study investigates wake development behind yawed turbines using large-eddy simulation (LES) with a rotating actuator disk model (ADM-R) under uniform inflow and varying yaw angles. Section 2 outlines the simulation setup, Section 3 presents wake deformation and turbulence characteristics, and Section 3.2 focuses on yaw-driven redirection. Final conclusions are drawn in Section 4.

2 Numerical Methods

2.1 Governing Equations

Large-eddy simulations were carried out using the PALM model developed by IMUK [12], excluding gravity, Coriolis, and buoyancy forces to focus on the wake effects of yawed turbines. The incompressible Navier–Stokes equations for the ABL were solved:

$$\frac{\partial u_i}{\partial x_i} = 0, \tag{1}$$

$$\frac{\partial u_i}{\partial t} = -\frac{\partial (u_i u_j)}{\partial x_j} - \frac{1}{\rho_0}\frac{\partial \pi^*}{\partial x_i} - \frac{\partial}{\partial x_j}\left(\overline{u_i' u_j'} - \frac{2}{3} e \delta_{ij}\right), \tag{2}$$

where $x_i = (x, y, z)$ are Cartesian coordinates, and $u_i = (u, v, w)$ are the filtered velocity components. ρ_0 is air density, e is the SGS turbulent kinetic energy, and π^*

is the modified pressure. A predictor–corrector method solves for π^* using Poisson equation solutions [13].

Turbulence was modeled with PALM's dynamic SGS scheme, based on the revised Deardorff model [14]:

$$\overline{u_i' u_j'} - \frac{2}{3} e \delta_{ij} = -K_m \left(\frac{\partial u_i}{\partial x_j} + \frac{\partial u_j}{\partial x_i} \right), \tag{3}$$

$$K_m = c_s \, \Delta_{\text{max}} \sqrt{e}, \tag{4}$$

where $\Delta_{\text{max}} = \max(\Delta x, \Delta y, \Delta z)$ and c_s is calculated via the Heinz method [15] and Mokhtarpoor et al. [16]. Molecular viscosity was neglected due to the high Reynolds number.

A staggered grid was employed [12], using 5$^{\text{th}}$-order upwind finite-difference and 3$^{\text{rd}}$-order Runge–Kutta schemes for spatial and temporal discretization [17].

2.2 Wind Turbine Model

The wind turbine was modeled using the actuator disk model with rotation (ADM-R) in PALM. This approach calculates axial and tangential forces on the rotor disk, based on the rotor's rotation, as described by Wu and Porté-Agel [12, 18]. The forces are determined through blade element momentum theory and distributed over the rotor disk using a 3D Gaussian kernel [18]. Chord lengths and lift/drag coefficients were tabulated at the blade element centers.

The NREL 5 MW Reference Wind Turbine [19], a standard turbine used in both research and industry, was modeled in this study. Blade rotational speed followed the control algorithm from the NREL 5 MW reference [19]. Key specifications are provided in Table 1.

Table 1: Specifications of the NREL 5 MW Reference Wind Turbine [19]

Specification	Value	Specification	Value
Rated Power	5 MW	Rotor Diameter	126 m
Rotor Orientation	Upwind	Hub Height	90 m
Rated Rotor Speed	12.1 rpm	Rated Wind Speed	11.4 m/s

2.3 Simulation Set-Up

The LES domain, shown in Figure 1, has a size of $(L_x, L_y, L_z) = (24D, 6D, 6D)$ in the streamwise, spanwise, and vertical directions, with $D = 126$ m as the rotor diameter. The grid resolution, $\Delta/D = 0.03125$, results in $(n_x, n_y, n_z) = (768, 192, 192)$

and a total of 28,311,552 grid points, capturing the curled wake structure in close agreement with prior studies on wake deformation [4, 9].

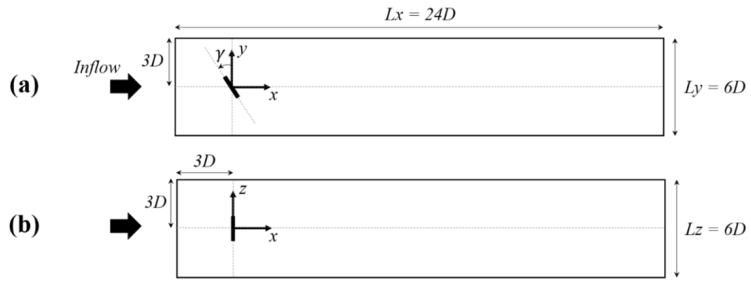

Figure 1: The simulation domain configuration: (a) top view, (b) side view.

The actuator disk (AD) was positioned $3D$ from the domain boundaries. The yaw angle (γ) was defined counterclockwise, and the rotor rotation was clockwise from the downstream view (Figure 1a). The hub, nacelle, and tower were excluded to isolate yaw-induced wake effects, as their inclusion slightly refines wake profiles but does not impact curled wake formation [20].

Boundary conditions included Dirichlet at the inlet, outflow at the outlet, and cyclic conditions in the y and z directions. A uniform inflow was used, excluding ground-induced shear to focus on yaw-induced wake curvature. Simulation cases with $U_\infty = 9\ \mathrm{m/s}$ and yaw angles from $-30°$ to $30°$ in $10°$ increments are summarized in Table 2.

Table 2: Simulation cases.

Inflow Wind Speed, U_∞ [m/s]	Yaw Angle, γ [°]
9	-30, -20, -10, 0, 10, 20, 30

3 Results and Discussion

3.1 Streamwise Velocity Fields and Turbulent Kinetic Energy

This section presents streamwise velocity, time-averaged streamlines, and turbulent kinetic energy (TKE) across yaw angles. TKE, k, is calculated as:

$$k = \frac{1}{2}\overline{u'^2 + v'^2 + w'^2} \tag{5}$$

Figure 2 shows $\overline{u}$ and k from $x/D = 1$ to 6 at $\gamma = 0°$. The wake stays circular until $x/D = 5$, with a velocity deficit mainly outside the hub. Streamlines follow the rotor's spin, and high k appears at the wake edge due to shear mixing.

At $\gamma = -20°$ (Figure 3), the wake becomes elliptical until $x/D = 2$ and shows a counter-rotating vortex pair (CVP) from $x/D = 1$. Downstream, it deforms into

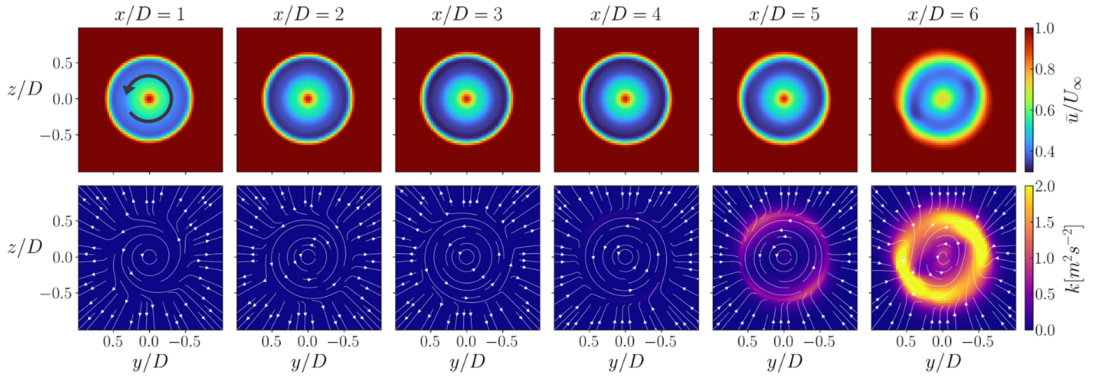

Figure 2: Mean velocity $\overline{u}$ and TKE k at $\gamma = 0°$. Streamlines (white); wake rotation (black arrow) [23].

a kidney shape [3, 4]. Wake rotation interacts with the CVP, increasing upper wake distortion and k around $x/D = 5$–6 due to upward mixing.

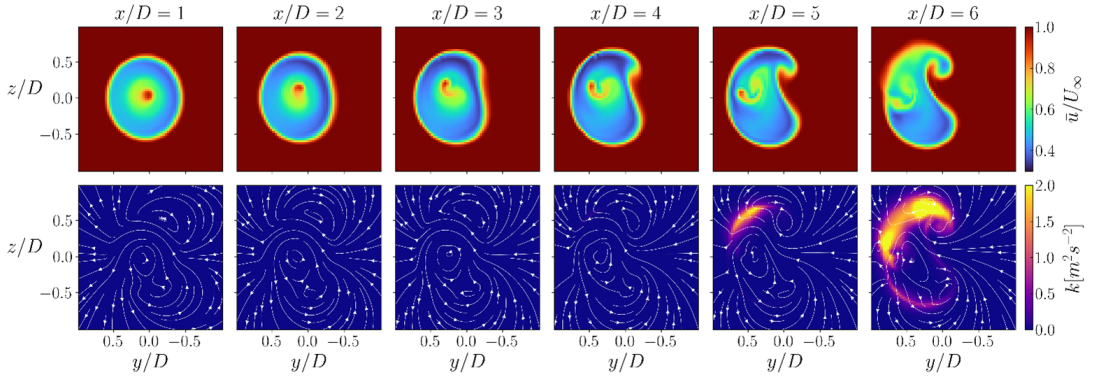

Figure 3: Contours of $\bar{u}$ and k at $\gamma = -20°$, time-averaged streamlines (white) [23].

Figure 4 shows vertical $\overline{u}$ profiles at $y = 0$ from $x/D = 3$ to 7 for $\gamma = \pm 20°$. Flipping the $-20°$ profile vertically aligns it with $+20°$, suggesting symmetric wake behavior, consistent with Kleusberg et al. [7]. Similar symmetry appears for $\gamma = \pm 30°$ (Figure 5).

3.2 Wake Centerlines and Skew Angles under Yaw

Wake centerlines were obtained via area-weighted average velocity deficit [3,21]. Figure 6 shows top-view contours of instantaneous u at $z = 0$ for $\gamma = 0°$ and $-20°$. Without yaw, the wake stays centered; with yaw, it deflects spanwise. Figure 7 reveals an additional downward shift, driven by shear–CVP interaction. Global wake rotation enhances upper CVP entrainment, shrinking the upper wake and displacing the centerline below the midplane.

Skew angles χ were calculated from the angle between the wake position vector $\vec{p}$

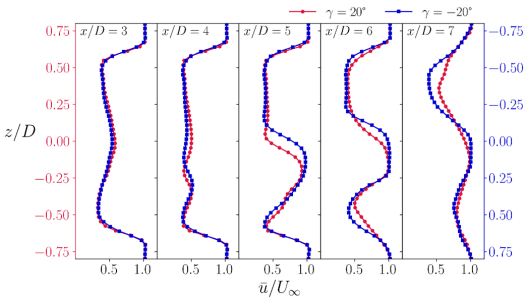

Figure 4: Vertical profiles of $\bar{u}$ at $y = 0$ for $\gamma = \pm 20°$ (red: $20°$, blue: $-20°$) [23].

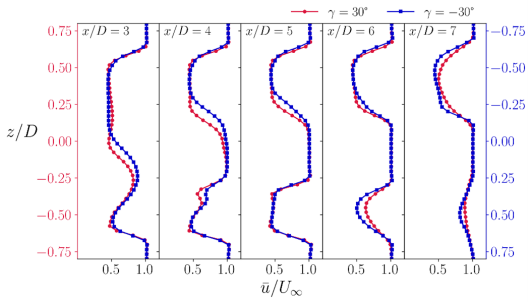

Figure 5: Vertical profiles of $\bar{u}$ at $y = 0$ for $\gamma = \pm 30°$ (red: $30°$, blue: $-30°$) [23].

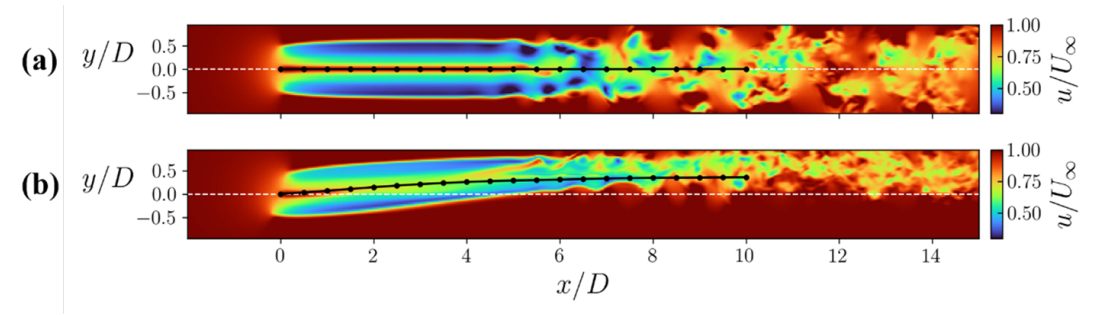

Figure 6: Instantaneous streamwise velocity u for (a) $\gamma = 0°$, (b) $\gamma = -20°$, with wake centerlines (black) [23].

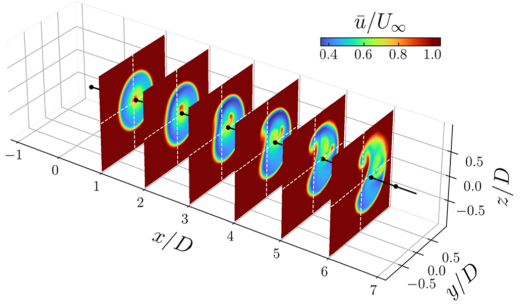

Figure 7: Time-averaged $\overline{u}$ at $\gamma = -20°$, with wake centerline (black) and domain centerlines ($y = 0$, $z = 0$, white dotted) [23].

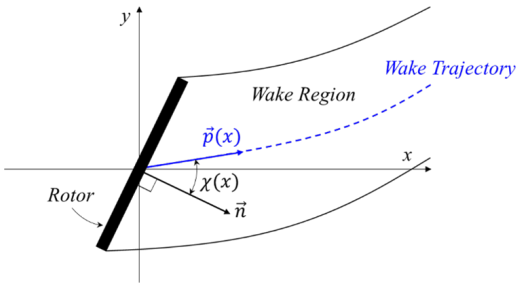

Figure 8: Definition of skew angle χ on the xy-plane.

and rotor normal $\vec{n}$ in the xy-plane (Figure 8, Equation (6)) [22]:

$$\chi(x) = \cos^{-1}\left(\frac{\vec{p}(x) \cdot \vec{n}}{\|\vec{p}(x)\| \, \|\vec{n}\|}\right) \tag{6}$$

4 Conclusions

This study examined the curled wake structure behind a yawed NREL 5 MW wind turbine under uniform inflow ($U_\infty = 9\ \mathrm{m/s}$) using LES. The turbine, modeled via a rotating actuator disk, was subjected to yaw angles $\gamma = -30^\circ \sim 30^\circ$. Yawing deformed the circular wake into an elliptical shape near the rotor, transitioning into a kidney-like structure downstream, with shape transformation accelerating as yaw increased. This transition typically occurred around $x/D = 3 \sim 5$, followed by a rapid rise in turbulent kinetic energy due to wake breakdown. Notably, negative yaw angles intensified turbulence near the upper wake boundary. Increased yaw amplified wake deformation and deflection in the near wake, while reducing velocity deficit and TKE due to lower thrust. However, wake rotation visibly affected the skew angle at higher yaw angles.

Acknowledgements

The authors acknowledge the computing resources provided by the Korea Institute of Science and Technology Information (KISTI).

References

[1] M. Mechali, R. Barthelmie, S. Frandsen, L. Jensen, P.E. Rethore, "Wake effects at Horns Rev and their influence on energy production", EWEC, 1, 10–20, 2006.

[2] Á. Jiménez, A. Crespo, E. Migoya, "Application of a LES technique to characterize the wake deflection of a wind turbine in yaw", Wind Energy, 13, 559–572, 2010.

[3] M.F. Howland, J. Bossuyt, L.A. Martínez-Tossas, J. Meyers, C. Meneveau, "Wake structure in actuator disk models of wind turbines in yaw under uniform inflow conditions", J. Renew. Sustain. Energy, 8, 043301, 2016.

[4] M. Bastankhah, F. Porté-Agel, "Experimental and theoretical study of wind turbine wakes in yawed conditions", J. Fluid Mech., 806, 506–541, 2016.

[5] C.R. Shapiro, D.F. Gayme, C. Meneveau, "Generation and decay of counter-rotating vortices downstream of yawed wind turbines in the atmospheric boundary layer", J. Fluid Mech., 903, R2, 2020.

[6] J. Schottler, J. Bartl, F. Mühle, L. Sætran, J. Peinke, M. Hölling, "Wind tunnel experiments on wind turbine wakes in yaw: Redefining the wake width", Wind Energy Sci., 3, 257–273, 2018.

[7] E. Kleusberg, P. Schlatter, D.S. Henningson, "Parametric dependencies of the yawed wind-turbine wake development", Wind Energy, 23, 1367–1380, 2020.

[8] N. Hamilton, H. Suk Kang, C. Meneveau, R. Bayoán Cal, "Statistical analysis of kinetic energy entrainment in a model wind turbine array boundary layer", J. Renew. Sustain. Energy, 4, 063105, 2012.

[9] M. Lin, F. Porté-Agel, "Large-eddy simulation of yawed wind-turbine wakes: Comparisons with wind tunnel measurements and analytical wake models", Energies, 12, 4574, 2019.
[10] J. Bartl, F. Mühle, J. Schottler, L. Sætran, J. Peinke, M. Adaramola, M. Hölling, "Wind tunnel experiments on wind turbine wakes in yaw: Effects of inflow turbulence and shear", Wind Energy Sci., 3, 329–343, 2018.
[11] P. Hulsman, M. Wosnik, V. Petrović, M. Hölling, M. Kühn, "Development of a curled wake of a yawed wind turbine under turbulent and sheared inflow", Wind Energy Sci., 7, 237–257, 2022.
[12] B. Maronga, S. Banzhaf, C. Burmeister, T. Esch, R. Forkel, D. Frohlich, V. Fuka, K.F. Gehrke, J. Geletič, S. Giersch, et al., "Overview of the PALM model system 6.0", Geosci. Model Dev., 13, 1335–1372, 2020.
[13] A.N.A. Patrinos, A.L. Kistler, "A numerical study of the Chicago lake breeze", Bound.-Lay. Meteorol., 12, 93–123, 1977.
[14] J.W. Deardorff, "Stratocumulus-capped mixed layers derived from a three-dimensional model", Bound.-Lay. Meteorol., 18, 495–527, 1980.
[15] S. Heinz, "Realizability of dynamic subgrid-scale stress models via stochastic analysis", Monte Carlo Meth. Appl., 14, 311–329, 2008.
[16] R. Mokhtarpoor, S. Heinz, "Dynamic large eddy simulation: Stability via realizability", Phys. Fluids, 29, 105104, 2017.
[17] L.J. Wicker, W.C. Skamarock, "Time-splitting methods for elastic models using forward time schemes", Mon. Weather Rev., 130, 2088–2097, 2002.
[18] Y.T. Wu, F. Porté-Agel, "Large-eddy simulation of wind-turbine wakes: Evaluation of turbine parametrisations", Bound.-Layer Meteorol., 138, 345–366, 2011.
[19] J. Jonkman, S. Butterfield, W. Musial, G. Scott, "Definition of a 5-MW Reference Wind Turbine for Offshore System Development", NREL/TP-500-38060, National Renewable Energy Laboratory, Golden, CO, USA, 2009.
[20] R.J. Stevens, L.A. Martínez-Tossas, C. Meneveau, "Comparison of wind farm large eddy simulations using actuator disk and actuator line models with wind tunnel experiments", Renew. Energy, 116, 470–478, 2018.
[21] M. Bastankhah, F. Porté-Agel, "Wind tunnel study of the wind turbine interaction with a boundary-layer flow: Upwind region, turbine performance, and wake region", Phys. Fluids, 29, 065105, 2017.
[22] S. Macrì, O. Coupiac, N. Girard, A. Leroy, S. Aubrun, "Experimental analysis of the wake dynamics of a modelled wind turbine during yaw manoeuvres", J. Phys. Conf. Ser., 1037, 072035, 2018.
[23] H. Kim, S. Lee, "Large Eddy Simulation of Yawed Wind Turbine Wake Deformation," Energies, 15(17), 6125, 2022.